9
Simulating Adsorption of Alkanes in Zeolites

Berend Smit and Rajamani Krishna
University of Amsterdam, Amsterdam, The Netherlands

I. INTRODUCTION

A proper description of adsorption phenomena is essential in the design of zeolite-based separations and catalysis. Transport and chemical reactions of molecules within zeolites are also significantly influenced by their adsorption characteristics. Though experimental data on adsorption of pure components in various zeolites are available, experimental data on mixture adsorption are scarce (1–3) due to the difficulty of experimentation with mixtures. In order to interpret the experimentally observed product distributions from zeolite-catalyzed processes, we need insights into the energetics and siting of intermediate molecular species formed during the reaction; it is very difficult to obtain such information from experiments.

Molecular simulations, in conjunction with experiments, have played an important role in the past few years in developing our understanding of the relation between microscopic and macroscopic properties of guest molecules in zeolitic hosts (4). Molecular dynamics (MD), Monte Carlo (MC), transition state, and rare-event simulation techniques have been used to study adsorption and diffusion in zeolites (4–11). Though molecular simulations have been applied to calculate the adsorption characteristics of a variety of molecules in zeolites (4), we restrict our discussions to *alkanes*. The reasons for this narrowed focus are as follows: (a) description of alkane adsorption is of great importance in the petroleum and petrochemical industries for processes such as catalytic isomerization; (b) many experimental investigations are available for alkane adsorption and these provide validation of molecular simulation strategies; and (c) many new ideas and concepts for separation and reaction have emerged from simulation studies on alkanes, as we shall demonstrate later in this chapter. The reader is referred to the recent review of Fuchs and Cheetham (4) for entry points into the literature for simulation studies of other types of molecules (alkenes, aromatics, inorganic molecules, etc.).

In adsorption studies, one would like to know the number of moles, or molecules, adsorbed within a given mass of zeolite as a function of the pressure and temperature of the reservoir in contact with the zeolite. One approach would be to use MD to simulate the experimental situation, i.e., a zeolite crystal in contact with, say, the gas phase; see Fig. 1a. In the actual experiments the equilibration may take minutes or several hours, depending on the type of molecule. These equilibration times will be reflected in an MD simulation; 1 min of experimental time would translate to about 10^9 on a computer. In most cases we are not interested in the properties of the gas phase, yet a significant amount of the CPU time consumed for an MD simulation will be spent on simulating the gas phase. Another complicating factor is

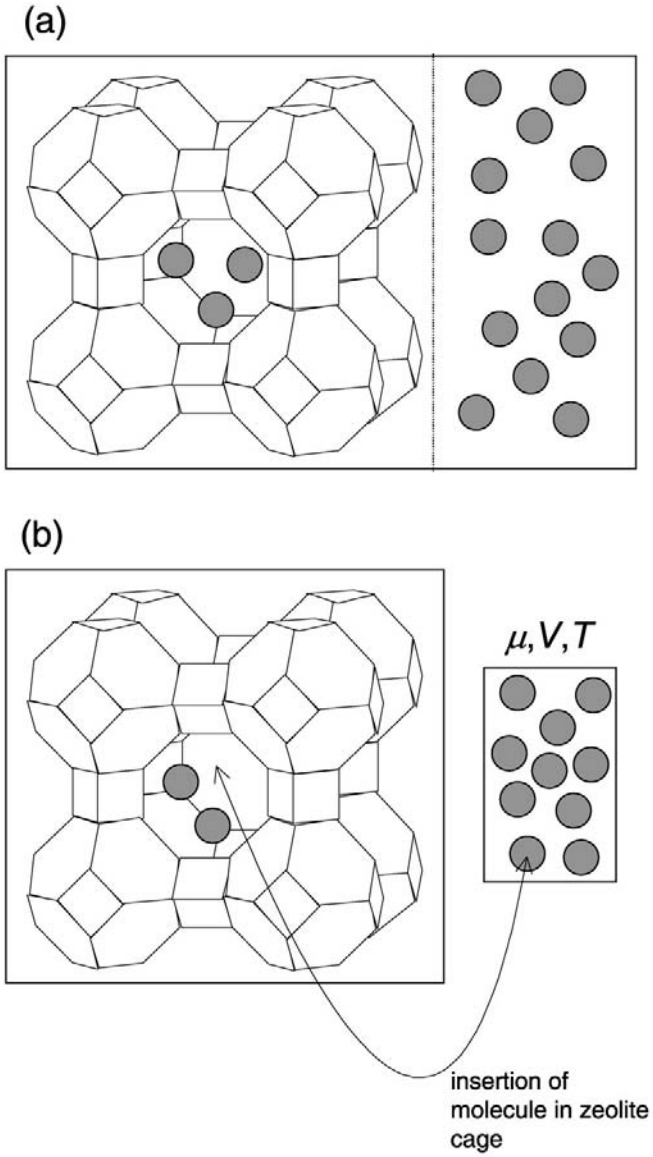

Fig. 1 Simulating adsorption of molecules in a zeolite using (a) molecular dynamics and (b) grandcanonical Monte Carlo techniques.

the proper modeling of the interface between the gas and the zeolite. Most of the aforementioned problems with MD simulations are circumvented by the use of MC simulations.

In MC simulations the zeolite crystals are allowed to exchange molecules with a reservoir of molecules at a fixed chemical potential in the grand canonical (or μ, *V*, *T*) ensemble; see Fig. 1b. In this ensemble, the temperature, volume, and chemical potential are fixed. The equilibrium conditions dictate that the temperature and chemical potential of fluid phase inside the zeolite and in the external reservoir must be equal. Therefore, we need to know only the μ and *T* of the gas in the reservoir in order to determine the equilibrium concentration of molecules

within the zeolite; this equilibrium is not affected in principle by the resistance of the gas–zeolite interface to transport of molecules. Care must be taken to compare equilibrium simulations with well-equilibrated adsorption measurements. In an MC simulation one does not have to follow the ''natural'' path of the molecule, as in a MD simulation, and one can perform ''moves'' to locate a molecule within an arbitrary position within the zeolite.

The naïve (unbiased) implementation of this technique works very well for small molecules such as methane. In an MC simulation for methane adsorption, we observe that of the 1000 attempts to place a methane molecule to a random position within a zeolite, 999 attempts will be rejected because the methane molecule overlaps with an atom the zeolite matrix. For ethane, only one move in 10^6 attempts will be successful. Clearly, the strategy of randomly inserting molecules within a zeolite matrix will not work for long-chain alkanes. To make MC simulations of long-chain molecules feasible, the configurational bias Monte Carlo (CBMC) technique has been developed (12). We first discuss the principles of the CBMC technique. Later, we show that CBMC simulations can provide new insights into the adsorption behaviors and provide clues to the development of novel separations relying on these insights.

II. CBMC SIMULATION TECHNIQUE

The principal idea of the CBMC technique is to grow an alkane chain, atom by atom, instead of attempting to insert the entire molecule at random. Figure 2 shows one of the steps in this algorithm; four atoms have been inserted successfully, and an attempt is made to insert the fifth. A number of candidate positions (denoted by arrows in Fig. 2) for insertion of the fifth atom are generated. Then one of the positions is selected in such a way that those trial positions with the lowest energy have the highest probability of being selected. Clearly a position that overlaps

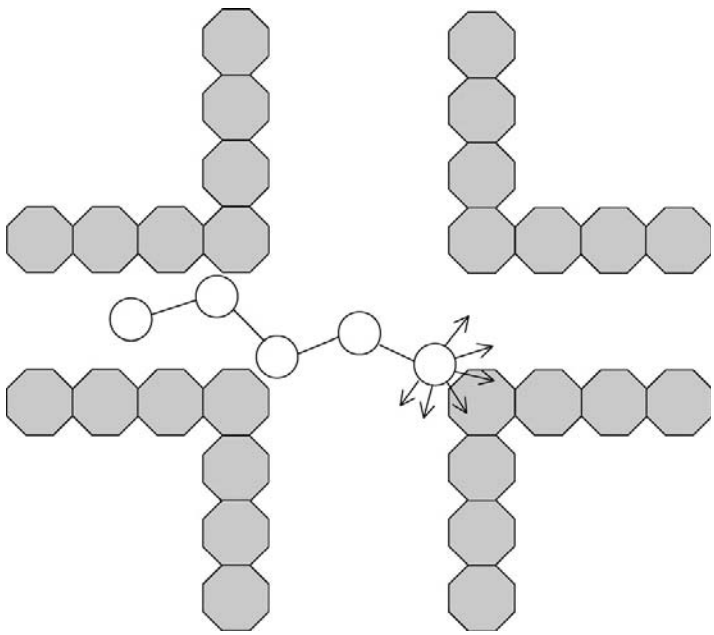

Fig. 2 Schematic drawing of the growing of an alkane in a zeolite in a CBMC move. The octagons represent the atoms of the zeolite and the circles represent the atoms of the alkane. Four atoms have been inserted successfully, and an attempt is made to insert the fifth.

with the zeolite structure is not an acceptable candidate. Important to note is that this growing procedure introduces a bias such that only the most favorable configurations are being generated. If one were to use the ordinary Metropolis acceptance rule, such a bias in the configurations of the molecules would lead to an incorrect distribution of configurations. This bias can be removed exactly by adjusting the acceptance rules (12). Computational details of the implementation of the CBMC algorithm are to be found in Vlugt et al. (13,14).

These simulations are performed in cycles and in each cycle an attempt to perform one of the following moves was made:

1. Displacement of a randomly selected chain.
2. Rotation of a chain around its center of mass.
3. Partly regrowing of a chain; a chain is selected at random and part of the molecule is regrown using the CBMC scheme.
4. Exchange with a reservoir; it is decided at random whether to add or to remove a molecule from the zeolite following the acceptance rules derived in Vlugt et al. (13,14).
5. Change of identity (only in the case of mixtures); one of the components is selected at random and an attempt is made to change its identity (13,14).

Typically the number of MC cycles performed is of order 10^7. Of these, about 15% are displacements, 15% rotations, 15% partial regrowths, 50% exchanges with the reservoir, and the remaining 5% of the moves were attempts to change the identity of a molecule. These probabilities can be further optimized depending on the details of the simulations.

A simple approach to describe the alkane molecules is to use the *united-atom model*, in which CH_3, CH_2, and CH groups are considered as single interaction centers. When these pseudoatoms belong to different molecules or to the same molecule but are separated by more than three bonds, the interaction is given by a Lennard-Jones potential. The Lennard-Jones parameters are chosen to reproduce the vapor–liquid curve of the phase diagram as shown in Siepmann et al. (15). The bonded interactions include bond bending and torsion potentials; details for the alkane model can be found in Vlugt et al. (13,14).

For the calculation of the adsorption isotherms of alkanes in silicalite, Macedonia and Maginn (16,17) have adopted a more detailed *all-atom model* to represent the alkanes. Both the *united-atom* model and the *all-atom* model gave comparable results for the prediction of adsorption of C_1–C_3 alkanes in silicalite (16,17).

Most simulation studies follow the approach of Kiselev and coworkers (18) and assume the zeolite lattice to be *rigid* and that interactions of an alkane with the zeolite are dominated by the dispersive forces between pseudo atoms of the alkane (within the framework of the united-atom description) and the oxygen atoms of the zeolite. These interactions have been described by a Lennard-Jones potential (13,14). Several authors have performed simulations on a flexible lattice [see the review by Demontis and Suffritti (5)]. These simulations show that a flexible lattice can influence the *diffusion* properties. To diffuse through the zeolite the molecules have to pass through narrow windows that form energy barriers. In a flexible zeolite one may observe fluctuations in the size of the window that could lower this energy barrier to a significant extent. However, for the calculation of *thermodynamic equilibrium* properties, the focus of the present chapter, such fluctuations in the window size would have a much less significant effect because these involve much lower energy barriers. Therefore, we expect that for simulation of adsorption isotherms of *alkanes* the use of a flexible zeolite would not change the results significantly. For simulating the adsorption of tight-fitting molecules in zeolitic hosts, it may be necessary to take account of lattice flexibility. Clark and Snurr (19) have studied the influence of lattice flexibility on the adsorption of benzene in silicalite and found that small changes in the zeolite structure can bring about large changes in the macroscopic behavior. For example, a difference of a factor of 3.1 in the Henry's law constant was observed.

A second aspect associated with the use of a flexible lattice is that the adsorbed molecule may induce a phase transition in the zeolite. Such a phase transition has been observed in H-ZSM5 for *p*-xylene (20), which molecules fit very snugly at the intersections of H-ZSM5. To the best of our knowledge such a transition has not been observed for linear and branched alkanes; this can be understood from the fact that alkanes do not have such a tight fit in silicalite. Put another way, the adsorption of linear and branched alkanes is not likely to induce phase transitions in the zeolite. A further implication is that the adsorption properties of alkanes are not very sensitive to the choice of the effective channel, or window, size within the zeolite matrix. The effective channel or window size is determined by the positions of the atoms of the zeolite matrix, as determined from the crystal structure, and the zeolite–alkane (e.g., Lennard-Jones) interactions. However, the recent work of Vlugt et al. (10) has shown that the choice of Lennard-Jones σ has a significant influence on the *diffusion* of isobutane in silicalite; this choice is of less critical importance for calculating adsorption isotherms (14).

For the CBMC simulations the required crystallographic data were obtained from the *Atlas of Zeolite Framework Types of the International Zeolite Association* (http://*www.iza-online.org/*).

We shall demonstrate in the following that CBMC simulations yield adsorption isotherms that are in *quantitative* agreement with experimental data. If one is interested in more *qualitative* aspects of adsorption, such as to study the effect of two competing adsorption sites on the shape of the adsorption isotherm, one may choose to use much simpler approaches such as lattice models (21,22).

III. SORPTION OF PURE ALKANES

The CBMC simulations of adsorption isotherms of pure components in zeolites usually fall into the type I or type IV category in the IUPAC classification (1). We consider first CBMC simulations for adsorption of alkanes in the one-to four-carbon-atom range in MFI zeolite

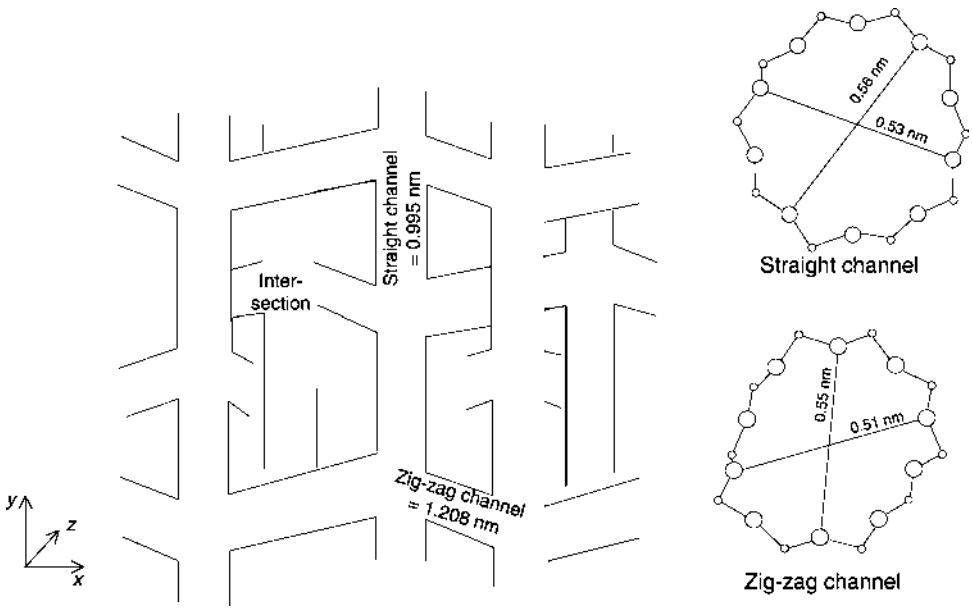

Fig. 3 Schematic structure of MFI (silicalite-1). The cross-sections of the straight and zig-zag channels are shown in the inset.

(silicalite-1) (23,24). Figure 3 shows a schematic of the structure of silicalite-1, which consists of a system of intersecting channels composed of zig-zag channels along x, cross-linked by straight channels along y. Both channels are defined by 10-rings. The straight channels are approximately elliptical in shape having a 0.53 nm × 0.56 nm cross-section while the zig-zag channels have a 0.51 × 0.55 nm cross-section; see Fig. 3. These length scales are obtained from crystallographic coordinates by calculating distances between oxygen atoms on opposite sides of channels and subtracting estimates of oxygen radii. The pure component isotherms at 300 K for methane, ethane, propane, and *n*-butane are shown in Fig. 4. Strictly speaking, the x axes of the data shown in Fig. 4 refer to the *fugacities* of the components, as these are the entities that are calculable from the chemical potentials that are used in grand canonical MC simulations. Nonideality effects come into play at very high pressures, and the appropriate equation of state needs to be used in order to determine the "corrected" pressures, as has been discussed by Vlugt et al. (23). The CBMC simulations are seen to be in very good agreement with the experimental data of Sun et al. (25) and Zhu et al. (26).

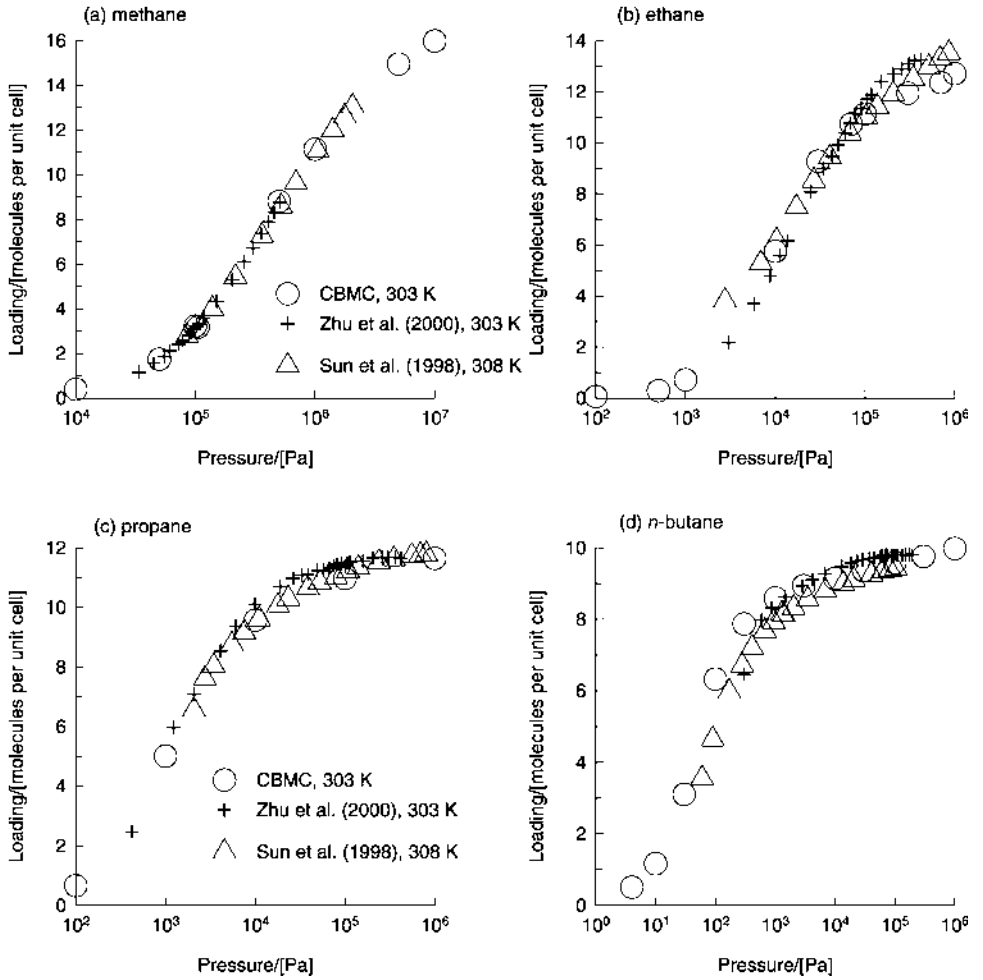

Fig. 4 Comparison of experimental data (Refs. 25,26) for pure component isotherms for (a) methane, (b) ethane, (c) propane, and (d) *n*-butane in MFI at 300 K with CBMC simulations (Refs. 23,24).

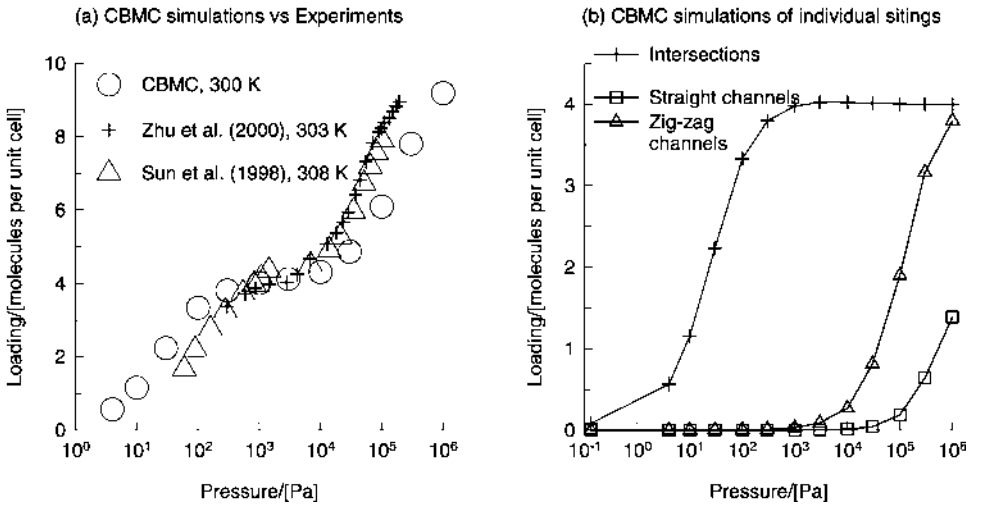

Fig. 5 (a) Comparison of experimental data (Refs. 25,26) for pure component isotherm for isobutane in MFI at 300 K with CBMC simulations (Refs. 23,24). (b) Loadings of isobutane at 300 K in intersection sites, straight channels, and zig-zag channels. The cutoff radius of sphere defining the intersection site is 0.3 nm. Simulation results from Ref. 24.

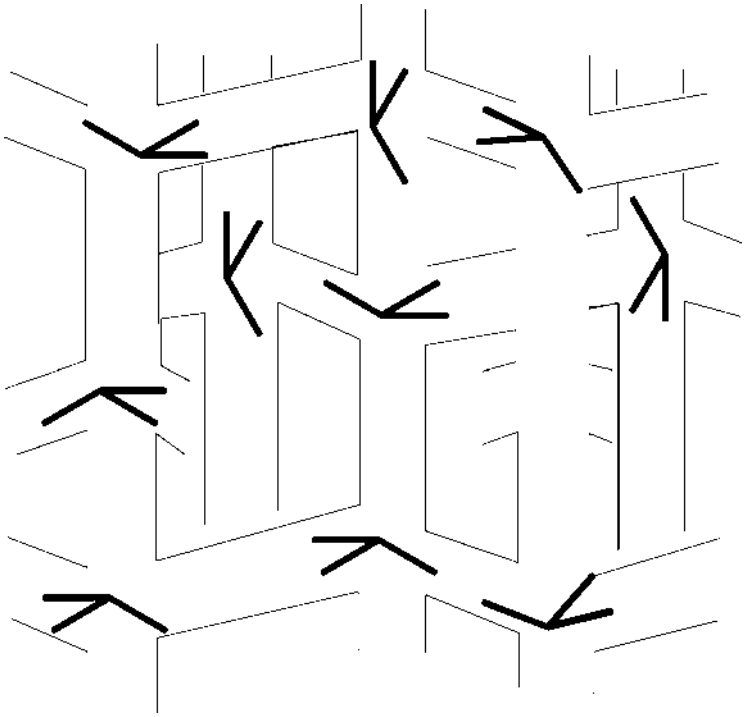

Fig. 6 Schematic showing preferential location of isobutane molecules at the intersections between the straight and zig-zag channels.

CBMC simulations provide much more insight into adsorption behavior than available from experiments alone. In order to illustrate this let us consider the experimental data for adsorption of isobutane in MFI at 300–303 K (25,26); the adsorption isotherm shows a pronounced inflection at a loading of four molecules per unit cell; see Fig. 5a. This inflection behavior is nicely reproduced by CBMC simulations. By actually counting the molecules in the various locations in the MFI structure, straight channels, zig-zag channels, and intersections we can develop the isotherms for each individual location; see Fig. 5b. It is clear from Fig. 5b that isobutane molecules prefer to locate at the intersections. Up to a system pressure of 1 kPa, the isobutane molecules are exclusively located at the intersections, which have a maximum capacity of four molecules per unit cell. This means that zeolite loadings in excess of four molecules per unit cell can only be achieved by pushing isobutane into the straight and zig-zag channels. Only when the pressure is significantly increased beyond 10 kPa do the zig-zag channels and straight channels tend to get occupied. Due to its branched configuration, isobutane demands an extra "push" to locate within these channels. This extra push is the root cause of the inflection behavior. Figure 6 shows a schematic of the siting of isobutane molecules within MFI.

All monobranched alkanes, in the five- to eight-carbon atom range are found to exhibit inflection behavior (14,27–30). Interestingly, *n*-hexane also shows a slight inflection at a loading of four molecules per unit [see, e.g., Fig. 7(a); this inflection is due to "commensurate freezing" (31) caused by the fact that the length of the *n*-hexane molecule is commensurate with the length of the zig-zag channel; see Fig. 7b.

Dibranched alkanes, typified by 2,2-dimethylbutane (22DMB), also prefer to locate at the intersections of MFI; see Fig. 8a. However, these molecules are much bulkier than monobranched alkanes and, consequently, they cannot be pushed into the channel interiors. The maximal loading of dibranched alkanes, such as 22DMB, in MFI is restricted to four molecules per unit cell; see Fig. 8b.

The inflection behavior of monobranched alkanes in MFI at a loading of four molecules per unit cell, as well as the restriction of the maximal loading of dibranched alkanes to this loading, is a consequence of configurational differences. This *configurational entropy* effect causes the molecular loadings of hexane isomers in MFI to follow the hierarchy linear > monobranched > dibranched.

With other zeolite structures the configurational entropy effects may act in a completely different manner. Consider the adsorption of hexane isomers *n*-hexane (nC6), 3-methyl pentane (3MP), and 22DMB in AFI. AFI is aluminophosphate $AlPO_4$-5 and has a different charge distribution than siliceous materials, such as silicalite-1, for which the potentials have been developed. Since it is assumed that the interactions with alkanes are dominated by the dispersive interaction with the O atoms of the zeolite, one may assume that to a first approximation the same parameters can be used. At present there are not enough experimental data to verify whether this assumption leads to sufficiently accurate results.

The CBMC simulations of the adsorption isotherms at 403 K are shown in Fig. 9. The adsorption hierarchy is found to be dibranched > monobranched > linear, which is opposite to the hierarchy for MFI. AFI consists of cylindrical channels of 0.73 nm diameter. The channel dimension is large enough to accommodate the bulky 22DMB and there is therefore no configurational penalty for these molecules. However, the length of the molecules decreases with increased degree of branching (Fig. 10); this implies that the number of molecules that can be accommodated into the channels increases with the degree of branching. The increased adsorption strength with increased branching can be termed a *length entropy* effect, arising as it does with decreasing linear dimension of the molecule. The *length entropy* effect has also been highlighted by Talbot (32) in a more general, but idealized, manner.

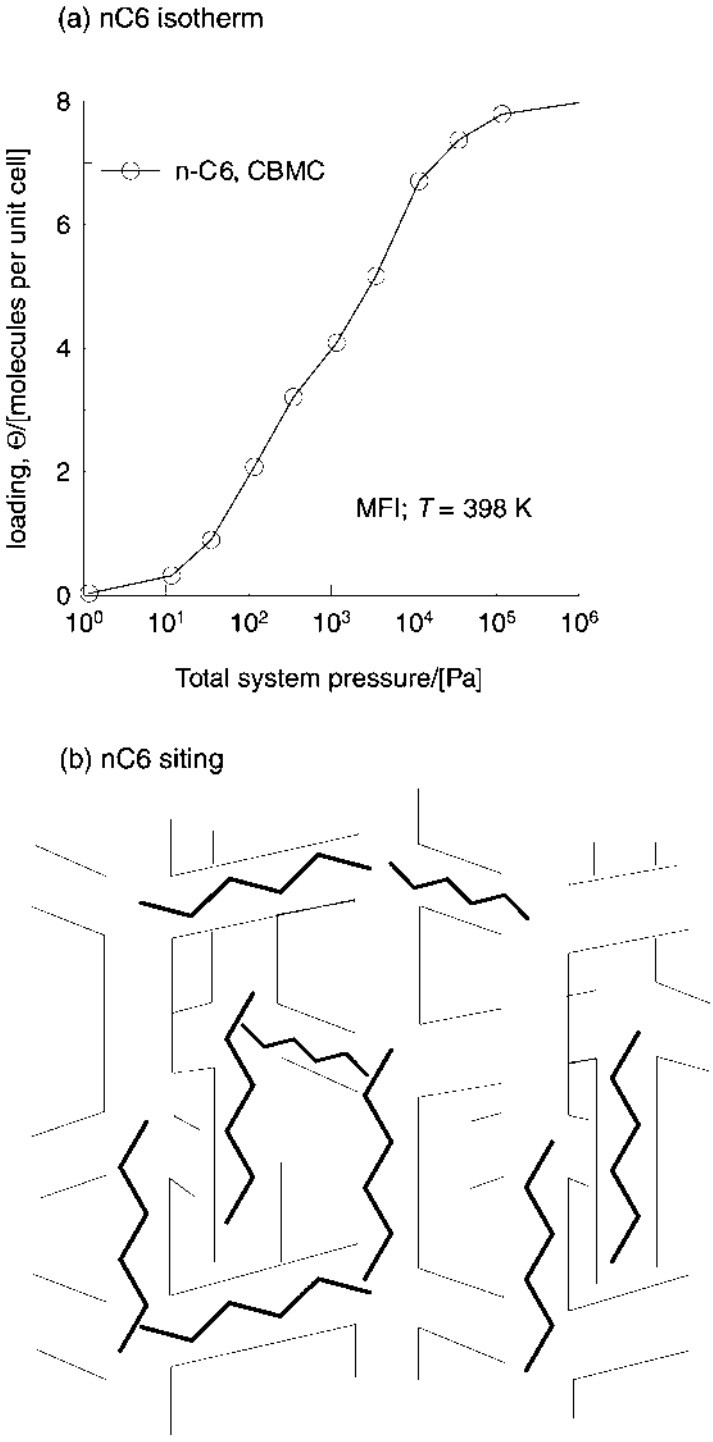

Fig. 7 (a) CBMC simulations of pure component isotherm for n = hexane in MFI at 398 K. (b) Schematic showing location of n-hexane molecules within MFI network.

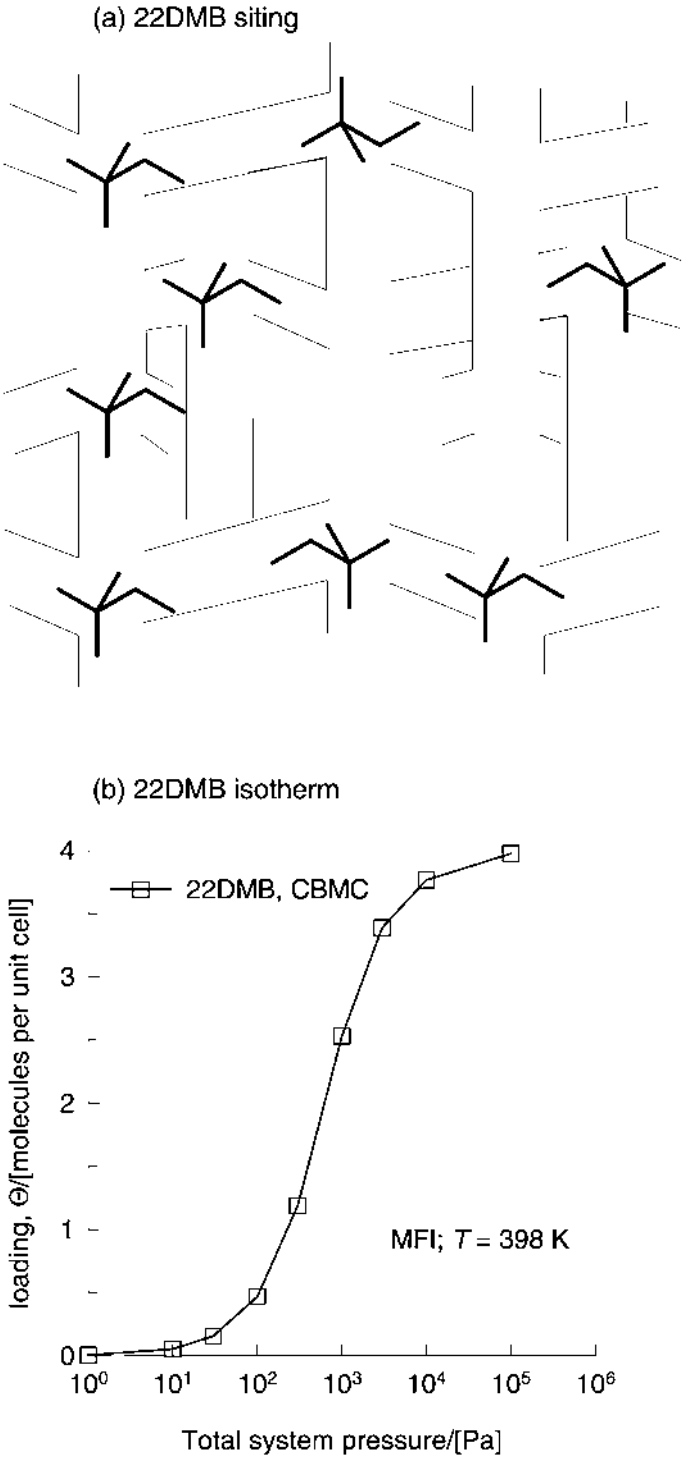

Fig. 8 (a) Schematic showing preferential location of 2,2-dimethylbutane (22DMB) at intersections between straight and zig-zag channels of MFI network. (b) CBMC simulations of pure component isotherm for 22DMB in MFI at 398 K.

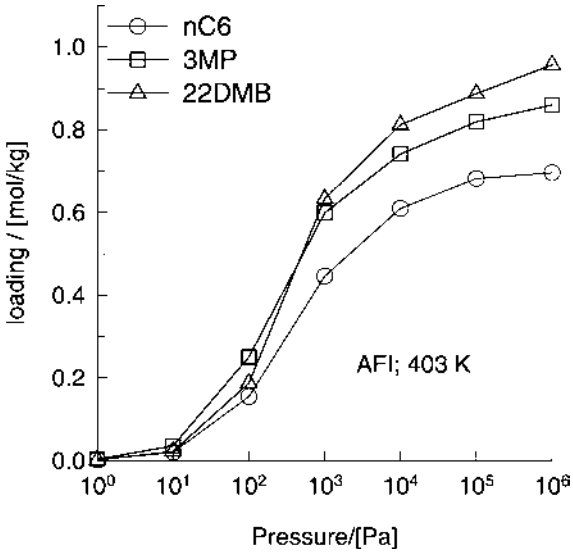

Fig. 9 Adsorption isotherms for nC6, 3MP, and 22DMB in AFI at 403 K determined by CBMC simulations.

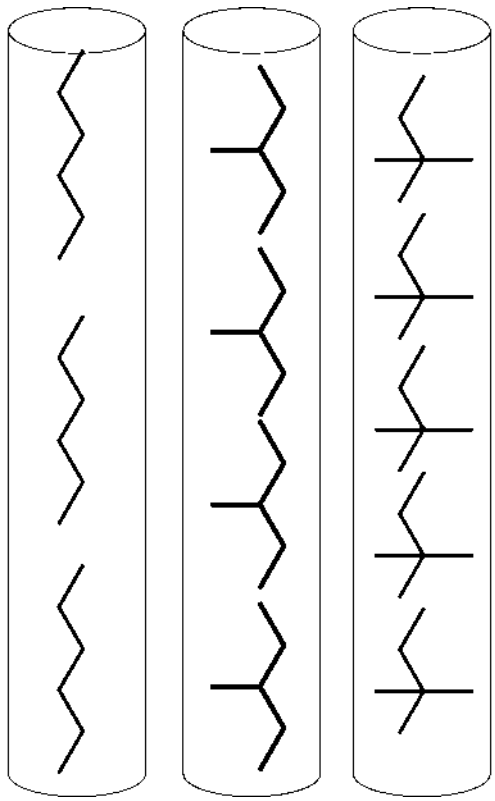

Fig. 10 Schematic of length entropy effect during adsorption of nC6, 3MP, and 22DMB in the cylindrical channels of AFI.

IV. SORPTION OF ALKANE MIXTURES

Almost all applications of adsorption involve mixtures (3), yet the number of experimental studies on adsorption of mixtures is very limited due to the difficulty of experimentation. Often in practice, the adsorption selectivity of mixtures is estimated on the basis of the values of the Henry coefficients, i.e., the adsorption strengths at near-zero loadings (33,34). For adsorption of alkanes in MFI at 300 K, the Henry coefficients, calculated from molecular simulations (14) are shown in Fig. 11; the Henry coefficients increase with increasing C number. We shall demonstrate below that using Henry coefficients to estimate the adsorption selectivity of *mixtures* is fraught with danger.

Let us first consider adsorption of an equimolar (50:50) mixture of C3 and nC4 in contact with MFI at 300 K. The component loadings obtained using CBMC simulations are shown in Fig. 12a. The loading of C3 increases continually with increasing pressure. On the other hand the loading of nC4 reaches a plateau value for pressures in the 10- to 100-kPa range. Increasing the total system pressure beyond 100 kPa leads to a *decline* in the loading of nC4! In Fig. 12b we plot the adsorption selectivity, which is the ratio of the loading of nC4 to that of C3.

For mixture loadings below 8, the adsorption selectivity of nC4 with respect to C3 is practically constant and equals that calculated from the corresponding Henry coefficients (from Fig. 11), i.e., 13. However, as the mixture loading increases beyond 8, the adsorption selectivity decreases dramatically to values just above unity. Near saturation loadings, the vacant spaces in the zeolite are more easily occupied by the smaller propane molecule. This is a manifestation of the *size entropy* effect that favors *smaller* molecules. It is clear that size entropy effects counter the effect of C number, which favors adsorption of the *larger* molecule.

MFI membrane permeation data of C1/C2, C1/C3, C2/C4, and C1/nC4 mixtures in the published literature (35–37) provide confirmation of the importance of size entropy effects at high loadings. As will be shown in Chapter 23 by Krishna, we need to take proper account of size entropy effects in order to model the membrane permeation data.

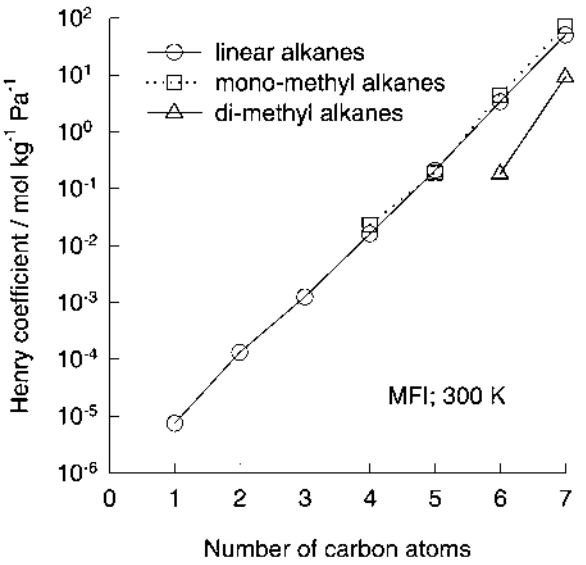

Fig. 11 Henry coefficients of alkanes in MFI at 300 K, calculated using CBMC simulations (from Ref. 14).

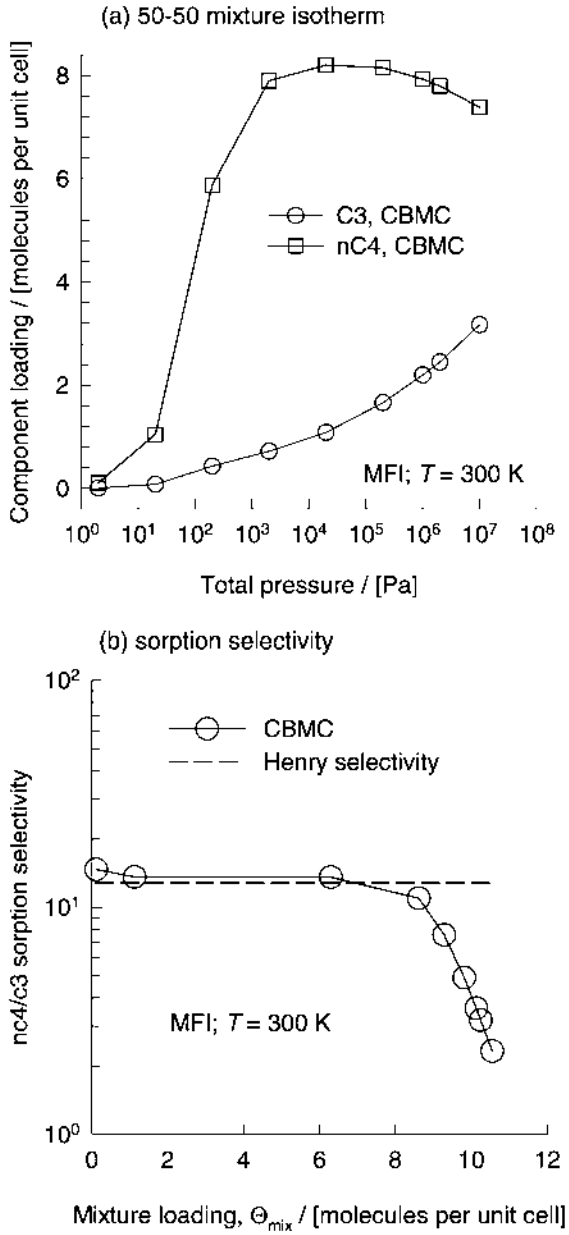

Fig. 12 (a) Adsorption loadings of equimolar binary mixture of C3 and nC4. (b) nC4/C3 adsorption selectivity.

Let us now consider the separation of hexane isomers, an important separation problem in the petroleum industry (34,38,39). Based on the adsorption selectivity in MFI dictated by the Henry coefficients (Fig. 11), we would conclude that it is not possible to separate the linear and the monobranched alkanes. In order to test this conclusion, let us consider CBMC simulations (14,27) for adsorption of a 50:50 mixture of nC6 and 3MP in MFI at a temperature 362 K. The component loadings in the mixture are shown in Fig. 13a for a range of pressures. It is

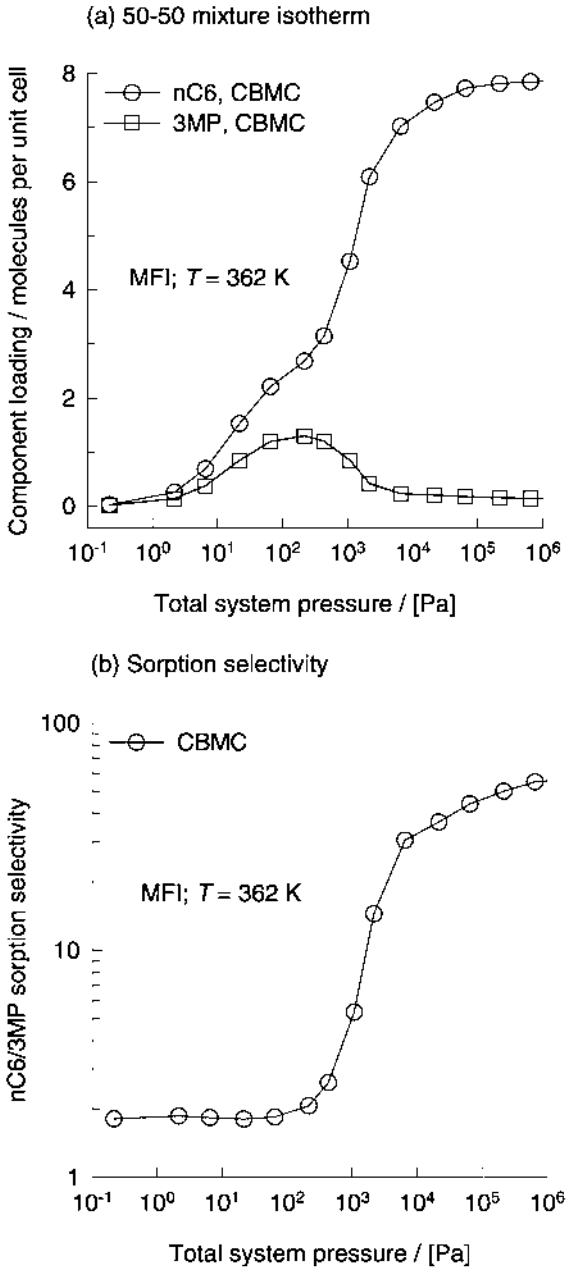

Fig. 13 (a) CBMC simulations of 50:50 mixture isotherm for nC6–3MP at 362 K in MFI. (b) Adsorption selectivity as a function of total system pressure.

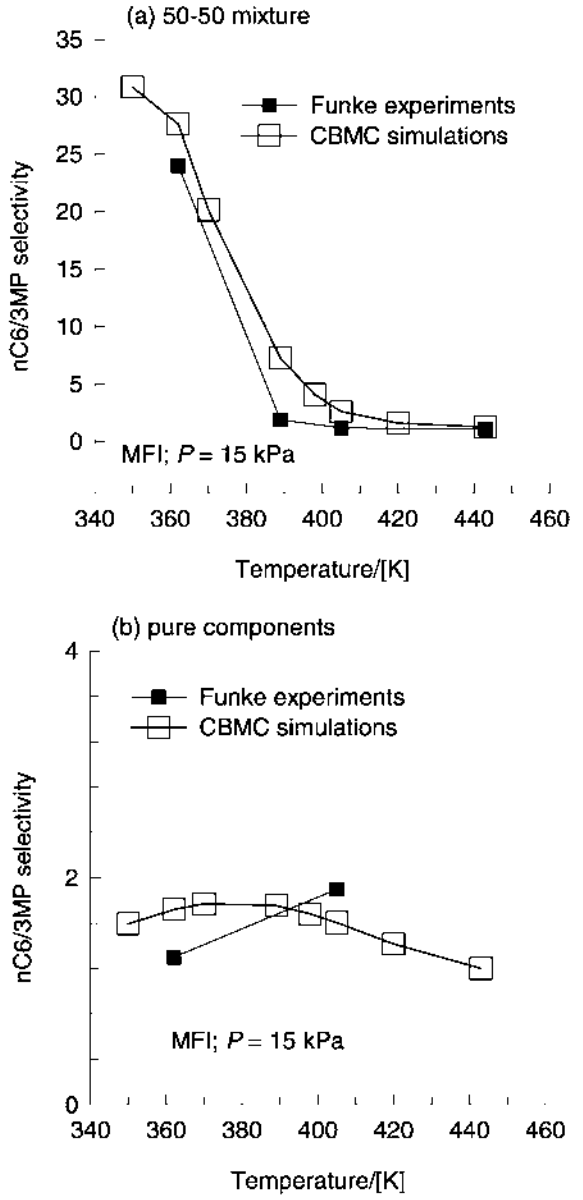

Fig. 14 (a) Adsorption selectivities calculated by CBMC simulations of 50:50 mixture of nC6–3MP at various temperatures in MFI, keeping the total pressure at 15 kPa. (b) Adsorption selectivities based on pure component loadings at various temperatures, keeping the total pressure at 15 kPa. Also shown are the experimentally determined membrane permeation selectivities of Funke et al. (Ref. 40).

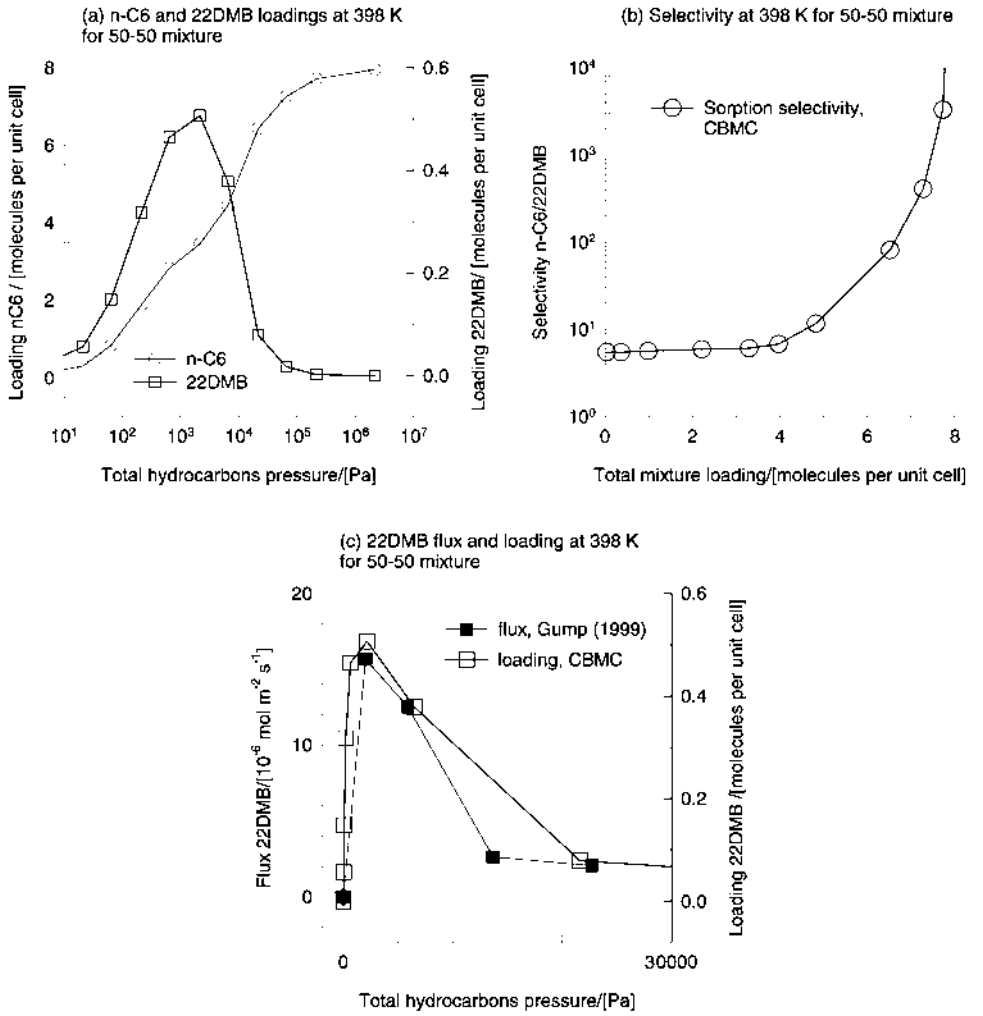

Fig. 15 (a) CBMC simulations of 50:50 mixture isotherm for nC6–22DMB at 398 K in MFI. (b) Adsorption selectivity as a function of total mixture loadings. (c) Comparison of loading of 22DMB with fluxes measured by Gump et al. (Ref. 41).

interesting to note the maximum in the loading of 3MP at about 100 Pa. When the pressure is raised above 100 Pa the loading of 3MP reduces virtually to zero. The nC6 molecules fit nicely into both straight and zig-zag channels (Fig. 7), whereas the 3MP molecules are preferentially located at the intersections between the straight channels and the zig-zag channels, as in the case of 22DMB (Fig. 8). Below a total loading of four molecules per unit cell, there is no real competition between nC6 and 3MP. The nC6 locates within the channels and 3MP at the intersections. When all the intersection sites are occupied, to further adsorb 3MP the system needs to provide an extra "push." Energetically, it is more efficient to obtain higher mixture loadings by "replacing" the 3MP with nC6; this *configurational entropy* effect is the reason behind the curious maximum in the 3MP loading in the mixture. The nC6/3MP adsorption selectivity is plotted in Fig. 13b. We see that the adsorption selectivity increases from near-unity values for pressures below 100 Pa to values of around 50 near saturation loadings.

Funke et al. (40) measured the permeation selectivities for 50:50 mixtures of nC6 and 3MP at various temperatures, keeping the upstream hydrocarbon pressure at 15 kPa; see Table 3 of their paper. At 362 K, they observed a membrane permeation selectivity for a 50:50 mixture S_P of 24 whereas S_P is 1.3 for the pure components. This high mixture selectivity can be explained by examination of Fig. 13b; the pressure of 15 kPa corresponds to conditions where there is a sharp increase in adsorption selectivity. The adsorption selectivity increases sharply beyond a total loading of four molecules per unit cell, corresponding to the situation in which all the intersections are occupied. Beyond this loading of 4, 3MP suffers a penalty from configurational entropy considerations and is practically excluded from the MFI matrix. The experimental permeation selectivities S_P, measured by Funke et al. (40), are compared with the adsorption selectivities S in a 50:50 mixture in Fig. 14a for a range of temperature conditions keeping the pressure constant at 15 kPa. The close agreement between the two sets of results confirms that configurational entropy effects are the cause of the high selectivities observed at lower temperatures. Such effects diminish with increasing temperatures, while the pressure is maintained constant at 15 kPa. The corresponding results for the selectivities based on pure component data is shown in Fig. 14b. Comparison of Fig. 14a and b underlines the danger of trying to estimate adsorption or membrane permeation selectivities for mixtures using pure component adsorption data.

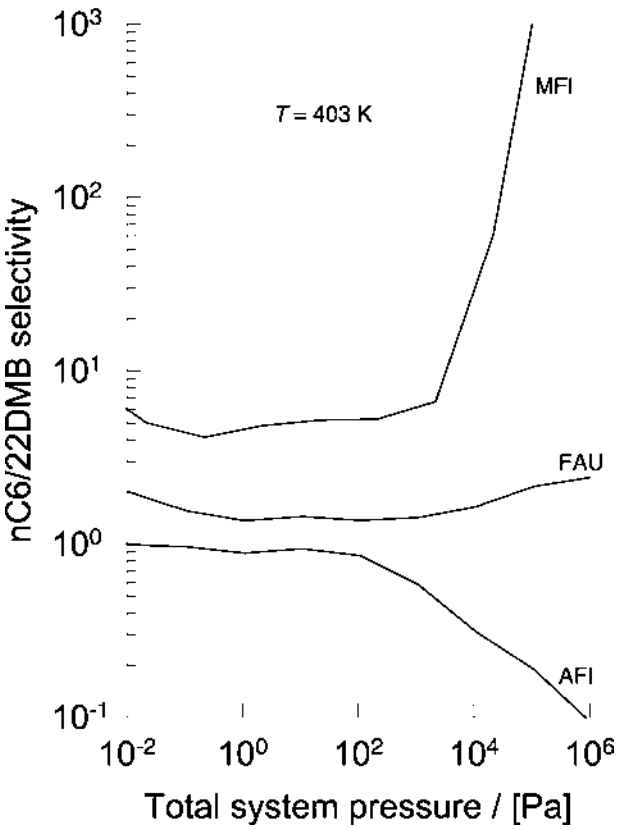

Fig. 16 CBMC simulations of adsorption selectivity in 50:50 mixture of nC6–22DMB at 403 K in MFI, FAU, and AFI.

Exactly analogous is the situation for adsorption of a mixture of nC6 and 22DMB; the component loadings at 398 K calculated with CBMC simulations are shown in Fig. 15a. We note that the double-branched isomer is virtually excluded at pressures exceeding 1 kPa due to configurational entropy effects. The adsorption selectivity increases dramatically beyond a total mixture loading of four molecules per unit cell; see Fig. 15b. A direct verification of the curious maximum in the component loading of 22DMB at a system pressure of 1 kPa is provided by the membrane permeation data of Gump et al. (41). Gump et al. reported the permeation fluxes of 50:50 mixtures of nC6 and 22DMB across a silicalite membrane at 398 K for various upstream hydrocarbon pressures; see figures 5 and 6 of their paper. Since the flux of any component is proportional to the loading at the upstream face, we would expect the flux of 22DMB to go through a maximum as the upstream compartment pressure is increased, in steps from 100 to 1000 Pa. This is precisely what Gump et al. (41) have observed in their experiments. The experimental fluxes of 22DMB are compared in Fig. 15c with the 22DMB loadings obtained from CBMC simulations. It is heartening to note that the experimentally observed maximal flux of 22DMB is obtained at the same pressure at which the 22DMB exhibits a maximum in its loading.

Our explanation of the membrane permeation experiments is different from that proposed by Funke et al. (40) and Gump et al. (41), who consider the *n*-hexane to effectively "block" the permeation of branched isomers. These authors do not offer an explanation of their membrane permeation experimental results in terms of the configurational entropy effects explained here.

The important message learned from the CBMC mixture simulations is that mixture adsorption, especially at high loadings, is significantly influenced by interactions between different species in the mixture, manifested by entropy effects. Ignoring entropy effects will cause us to pass up some important and interesting separation possibilities.

Molecular simulations can also help us to screen promising zeolite structures for a given separation task. For the separation of a 50:50 mixture of nC6 and 22DMB, the adsorption selectivity in three different zeolite topologies—MFI, FAU, and AFI—are shown in Fig. 16. In FAU, which has large cages, entropy effects do not come into play and the separation selectivity is about unity over the whole pressure range. In MFI, configurational entropy effects penalize 22DMB at high pressure (mixture loadings exceeding four molecules per unit cell), leading to high selectivities favoring the linear isomer. In AFI, consisting of straight cylindrical channels, length entropy effects (see also Fig. 10) favor 22DMB at high pressures.

V. SHAPE SELECTIVITY IN ZEOLITE CATALYSIS

In commercial practice, high selectivity is usually more valuable than high activity (42). Due to the crystallographically defined, uniform pore size, zeolites show unique and high degrees of selectivities. The selectivity originates from the shape (or configuration) of the particular guest molecules *and* the pore size and channel topology of the zeolitic hosts. It is usual to distinguish among three types of shape selectivities (42):

1. *Diffusion controlled.* It depends on the relative rates of diffusion of reactants and/or products, i.e., the kinetics of mass transfer.
2. *Sorption controlled.* The governing principle is the difference in the relative adsorption constants of the competing species, a thermodynamic rather than a kinetic property.
3. *Transition state controlled.* In systems where the intermediate or transition state of at least one of the reactions is larger than the reactants and products, the relative rate of competing reactions is influenced by the size of the pore size, and topology, of the zeolite.

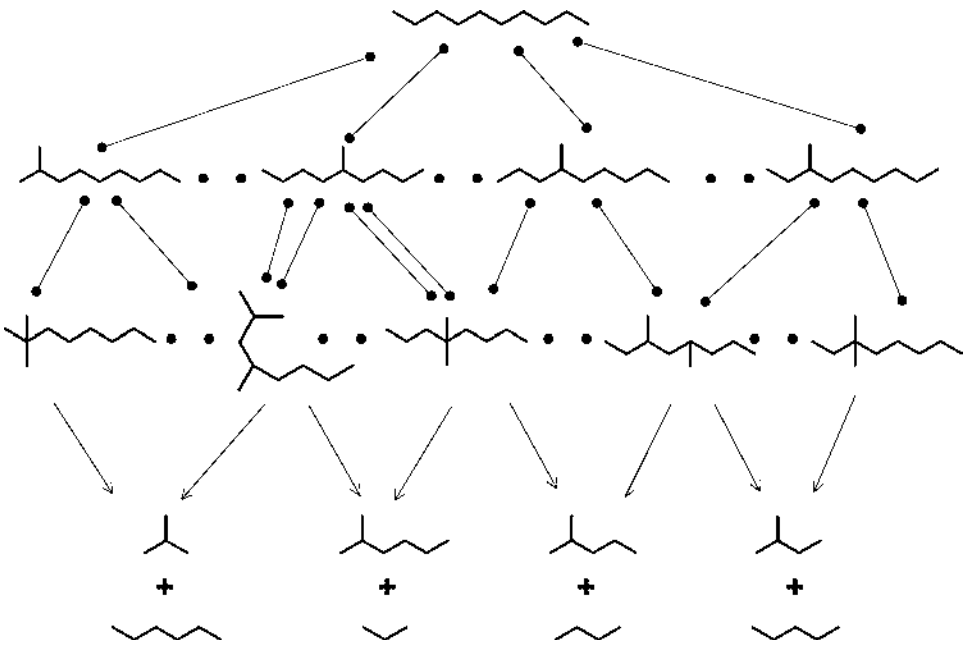

Fig. 17 Reaction pathways during hydrocracking of n-C10. Equilibration between isomers is denoted by lines with black dots at either end. Hydrocracking is denoted by arrows. As the methyl nonanes can hydroisomerize into 2,4-dimethyloctane and 4,4-dimethyloctane by three different routes, these two methyloctanes are kinetically favored. This is the simplified reaction scheme adapted from Maesen et al. (44).

The power of molecular simulations in rationalizing experimentally observed reaction pathways, and shape selectivity, has been demonstrated in the recent works of Maesen, Smit, and coworkers (43–45). In order to illustrate these ideas, let us consider the zeolite catalyzed hydrocracking of *n*-decane (nC10). The *n*C10 first undergoes hydroisomerization to a mixture of monobranched nonanes and dibranched decanes before getting cracked to linear and monomethyl paraffins; see Fig. 17.

It is clear that if the intermediate 2,4-dimethyoctane is favored in a particular zeolite catalyst, the reaction product would contain isobutane. On the other hand, if the intermediate 4,4-dimethyoctane is favored, the reaction product would contain *n*-butane.

Differences in the Gibbs free energy of formation of various reaction intermediates (shown in Fig. 17) determine the equilibrium concentration of reaction intermediates. If we use the tabulated free energies in the gas phase, we would predict that all reaction pathways shown in Fig. 17 are of comparable importance and that all of the alkanes shown at the bottom of Fig. 17 will form. Maesen et al. (43–45) used CBMC techniques to determine the free energies of formation in various zeolites. These CBMC calculations are shown in Fig. 18 for the important reaction intermediates for nC10 hydrocracking; the free energies are calculated for individual molecules, relative to nC10. We note that for large-pore FAU the free energies of formation relative to nC10 of the various reaction intermediates are virtually identical; this zeolite does not distinguish between the various species, and the complete spectrum of products shown in Fig. 17 is obtained in practice. Put another way, the large-pore FAU does not differentiate between the reaction intermediates because all of these can enter and occupy the FAU cages with equal ease.

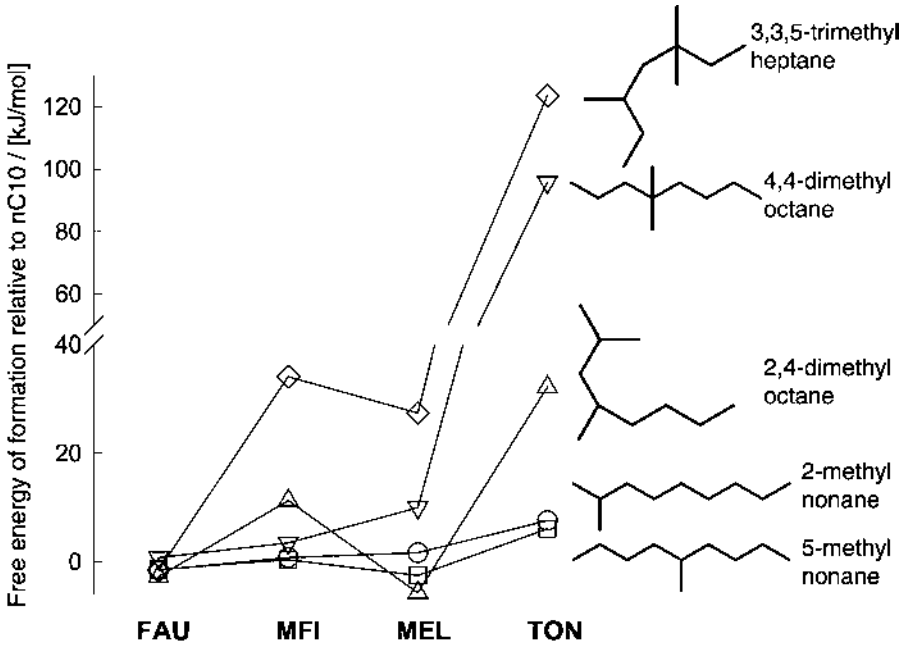

Fig. 18 The Gibbs free energy of formation of 2-methylnonane, 5-methylnonane, 2,4-dimethyloctane, 4,4-dimethyloctane, and 3,3,5-trimethylheptane, relative to *n*-decane in the zeolites FAU, TON, MFI, and MEL. Calculations from CBMC simulations (Refs. 44 and 45).

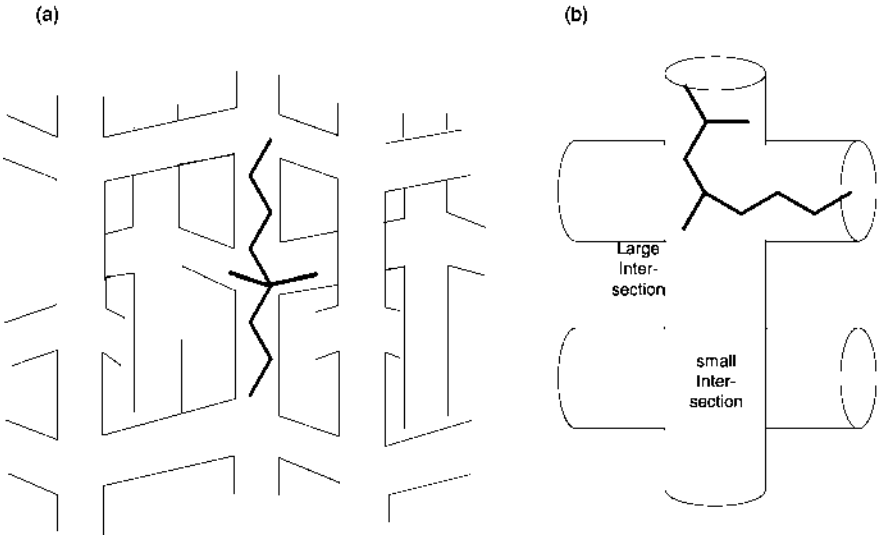

Fig. 19 (a) Siting of 4,4-dimethyloctane within MFI. (b) Siting of 2,4-dimethyloctane in MEL.

The situation changes dramatically when we consider zeolites with smaller pore dimensions such as MFI, MEL, and TON. In MFI, MEL, and TON we observe large differences in the Gibbs free energy between the reaction intermediates. For example, the Gibbs free energy of formation of the tribranched 3,3,5-trimethylheptane, with proximate methyl groups, is large. The formation of these isomers will therefore be suppressed.

Of the dimethyloctanes which are possible reaction intermediates (see Fig. 17), those with methyl groups attached to the same C atom or separated by one methylene (-CH_2-) group hydrocrack more easily than the other dimethyloctanes; this is because they form secondary and tertiary carbocation transition states instead of only secondary carbocation transition states. Thus, 2,4-dimethyloctane and 4,4-dimethyloctane are the more reactive intermediates. We note from Fig. 18 that the free energy of formation of these two molecules is higher in TON than in MFI or MEL. This is the reason for the higher hydrocracking activity of MFI and MEL relative to TON. Another interesting observation is that the free energy of formation of 4,4-dimethyloctane is lower in MFI than in MEL. This can be explained from the ease with which 4,4-dimethyloctane can be located within the MFI matrix. As can be seen from Fig. 19a, the octane backbone occupies the straight channels and two methyl groups protrude into the two zig-zag channels. The MEL structure consists of large and small intersections. The large intersections, formed by the channels that are perpendicular to each other, provide a perfect fit for the 2,4-dimethyloctane molecule; see Fig. 19b. Since hydrocracking of 2,4-dimethyloctane yields isobutane, whereas hydrocracking of 4,4-dimethyloctane yields *n*-butane (see reaction scheme in Fig. 17), we can rationalize why hydroconversion on nC10 using MEL yields twice as much isobutane as that using MFI-type zeolites (43–45).

VI. CONCLUDING REMARKS

In this chapter we have shown the demonstrated the power of CBMC simulations in determining the adsorption isotherms for pure alkanes and their mixtures in various zeolites. Besides providing useful data for zeolite process design, molecular simulations provide insights not possible by experiments alone. The inflection in the isotherm of branched alkanes in MFI is due to preferential location at the intersections between straight and zig-zag channels. CBMC simulations also help to highlight subtle entropy effects. For binary mixtures of linear alkanes, size entropy effects come into play at high mixture loadings and these counteract chain length effects to reduce separation selectivities; see Fig. 12. The molecule of the smaller size is preferentially adsorbed at high loadings because the few empty voids can be more easily filled. For adsorption of linear and monobranched isomers in MFI the selectivity increases in favor of the linear isomer for mixture loadings greater than 4; see Fig. 13. This is due to configurational entropy effects. This effect is so strong that the monobranched alkanes are virtually excluded from the MFI matrix at saturation loadings. For binary mixtures of linear and dibranched isomers in MFI, the adsorption selectivity is strongly in favor of the linear isomer; no branched isomer is adsorbed for mixture loadings greater than 4 (see Fig. 15). This is again due to configurational entropy effects. There is experimental verification of the importance of entropy effects during membrane permeation (35–37,40,41). The entropy concept can be exploited in practice to separate a mixture of linear and branched isomers in the five-to seven-carbon-atom range (29).

In AFI zeolites, the length entropy effect comes into play, and this favors the adsorption of the double-branched isomer; see Fig. 10.

For any separation task, CBMC simulations can be used to screen promising zeolite structures on the basis of their adsorption selectivities; see, e.g., 16. The more conventionally used method of using Henry coefficients to screen zeolites is fraught with danger because it does not reflect the subtle entropy effects that manifest at higher loadings.

CBMC simulations can also be used to throw light on the shape selectivity in catalysis. By determining the free energy of formation of reaction intermediates in various zeolites using CBMC techniques, we can rationalize experimentally observed product distributions. A more tantalizing prospect is the use of CBMC simulations to screen zeolite structures on the basis of their reaction selectivities.

ACKNOWLEDGMENTS

The authors gratefully acknowledge grants from the Netherlands Organization for Scientific Research (NWO-CW).

REFERENCES

1. DM Ruthven. Principles of Adsorption and Adsorption Processes. New York: Wiley, 1984.
2. J Kärger, DM Ruthven. Diffusion in Zeolites and Other Microporous Solids. New York: Wiley, 1992.
3. O Talu. Needs, status, techniques and problems with binary gas adsorption experiments. Adv Colloid Interf Sci, 76–77:227–269, 1998.
4. AH Fuchs, AK Cheetham. Adsorption of guest molecules in zeolitic materials: computational aspects. J Phys Chem B 105:7375–7383, 2001.
5. P Demontis, GB Suffritti. Structure and dynamics of zeolites investigated by molecular dynamics. Chem Rev 97:2845–2878, 1997.
6. B Smit, LDJC Loyens, GLMM Verbist. Simulation of adsorption and diffusion of hydrocarbons in zeolites. Faraday Disc 106:93–104, 1997.
7. C Tunca, DM Ford. A transition-state theory approach to adsorbate dynamics at arbitrary loadings. J Chem Phys 111:2751–2760, 1999.
8. SM Auerbach. Theory and simulation of jump dynamics, diffusion and phase equilibrium in nanopores. Int Rev Phys Chem 19:155–198, 2000.
9. FJ Keil, R Krishna, MO Coppens. Modeling of diffusion in zeolites. Rev Chem Eng 16:71–197, 2000.
10. TJH Vlugt, C Dellago, B Smit. Diffusion of isobutane in silicalite studied by transition state sampling. J Chem Phys 113:8791–8799, 2000.
11. B Smit, R Krishna. Monte Carlo simulations in zeolites. Curr Opin Solid State Microsc 5:455–461, 2001.
12. D Frenkel, B Smit. Understanding Molecular Simulations: From Algorithms to Applications, 2nd ed. San Diego: Academic Press, 2002.
13. TJH Vlugt, MG Martin, JI Siepmann, B Smit, R Krishna. Improving the efficiency of the CBMC algorithm. Mol Phys 94:727–733, 1998.
14. TJH Vlugt, R Krishna, B Smit. Molecular simulations of adsorption isotherms of linear and branched alkanes and their mixtures in silicalite. J Phys Chem B 103:1102–1118, 1999.
15. JI Siepmann, MG Martin, CJ Mundy, ML Klein. Intermolecular potentials for branched alkanes and the vapor-liquid phase equilibria of n-heptane, 2-methylhexane, and 3-ethylpentane. Mol Phys 90:687–693, 1997.
16. MD Macedonia, EJ Maginn. Pure and binary sorption equilibria of light hydrocarbons in the zeolite silicalite from grand canonical Monte Carlo simulations. Fluid Phase Equilibr 158-160: 19–27, 1999.
17. MD Macedonia, EJ Maginn. A biased grand canonical Monte Carlo method for simulating adsorption using all-atom and branched united atom models. Mol Phys 96:1375–1390, 1999.

18. AG Bezus, AV Kiselev, AA Lopatkin, PQ Du. Molecular statistical calculation of the thermodynamic adsorption characteristics of zeolites using the atom-atom approximation. Part 1. Adsorption of methane by zeolite sodium-X. J Chem Soc Faraday Trans II 74:367–379, 1978.
19. LA Clark, RQ Snurr. Adsorption isotherm selectivity to small changes in zeolite structure. Chem Phys Lett 308:155–159, 1999.
20. H Van Koningsveld, F Tuinstra, H Van Bekkum, JC Jansen. The location of para-xylene in a single cryst of zeolite H-ZSM-5 with a new, sorbate-induced, orthorhombic framework symmetry. Acta Crystallogr B 45:423–431, 1989.
21. PR Van Tassel, HT Davis, AV McCormick. New lattice model for adsorption of small molecules in zeolite micropores, AIChE J 40:925–934, 1994.
22. G Manos, LJ Dunne, MF Chaplin, ZM Du. Comparative study of Monte Carlo simulations and exact statistical mechanical lattice model of commensurate transitions of alkanes adsorbed in zeolites. Chem Phys Lett 335:77–84, 2001.
23. TJH Vlugt, W Zhu, F Kapteijn, JA Moulijn, B Smit, R Krishna. Adsorption of linear and branched alkanes in the zeolite silicalite-1. J Am Chem Soc 120:5599–5600, 1998.
24. R Krishna, D Paschek. Molecular simulations of adsorption and siting of light alkanes in silicalite-1. Phys Chem Chem Phys 3:453–462, 2001.
25. MS Sun, DB Shah, HH Xu, O Talu. Adsorption equilibria of C1–C4 alkanes, CO_2 and SF_6 on silicalite. J Phys Chem B 102:1466–1473, 1998.
26. W Zhu, F Kapteijn, JA Moulijn. Adsorption of light alkanes in silicalite-1: reconciliation of experimental data and molecular simulations. Phys Chem Chem Phys 2:1989–1995, 2000.
27. M Schenk, SL Vidal, TJH Vlugt, B Smit, R Krishna. Separation of alkane isomers by exploiting entropy effects during adsorption on silicalite-1: A configurational-bias Monte Carlo simulation study. Langmuir 17:1558–1570, 2001.
28. S Calero, B Smit, R Krishna. Separation of linear, mono-methyl and di-methyl alkanes in the 5- 7 carbon atom range by exploiting configurational entropy effects during sorption on silicalite-1. Phys Chem Chem Phys 3:4390–4398, 2001.
29. R Krishna, B Smit, TJH Vlugt. Sorption-induced diffusion-selective separation of hydrocarbon isomers using silicalite. J Phys Chem A 102:7727–7730, 1998.
30. R Krishna, B Smit, S Calero. Entropy effects during sorption of alkanes in zeolites. Chem Soc Rev 31:185–194, 2002.
31. B Smit, TLM Maesen. Commensurate "freezing" of alkanes in the channels of a zeolite. Nature 374:42–44, 1995.
32. J Talbot. Analysis of adsorption selectivity in a one-dimensional model system. AIChEJ 43:2471–2478, 1997.
33. JF Denayer, GV Baron, JA Martens, PA Jacobs. Chromatographic study of adsorption of n-alkanes on zeolites at high temperatures. J Phys Chem B 102:3077–3081, 1998.
34. K Huddersman, M Klimczyk. Separation of branched hexane isomers using zeolite molecular sieves. AIChEJ 42:405–408, 1996.
35. J Van de Graaf, F Kapteijn, JA Moulijn. Modeling permeation of binary mixtures through zeolite membranes. AIChEJ 45:497–511, 1999.
36. F Kapteijn, JA Moulijn, R Krishna. The generalized Maxwell-Stefan model for diffusion in zeolites: sorbate molecules with different saturation loadings. Chem Eng Sci 55:2923–2930, 2000.
37. WJW Bakker. Structured systems in gas separation. PhD dissertation, Delft University of Technology, 1999.
38. RS Haizmann, FM Hibbs, S Raghuram. Integrated isomerization and adsorption steps for upgrading C5 and C6 hydrocarbons, US Patent 5043525 to UOP, Inc., 1993.
39. HW Dandekar, GA Funk, HA Zinnen. Process for separating and recovering multimethyl-branched alkanes, US Patent 6069289 to UOP, Inc., 2000.
40. HH Funke, AM Argo, JL Falconer, RM Noble. Separation of cyclic, branched, and linear hydrocarbon mixtures through silicalite membranes. Ind Eng Chem Res 36:137–143, 1997.

41. CJ Gump, RD Noble, JL Falconer. Separation of hexane isomers through nonzeolite pores in ZSM-5 zeolite membranes. Ind Eng Chem Res 38:2775–2781, 1999.
42. WO Haag. Catalysis by zeolites—science and technology. Zeolites and related microporous materials: state of the art 1994, Part A–C. Stud Surf Sci Catal 84:1375–1394, 1994.
43. TLM Maesen, M Schenk, TJH Vlugt, JP de Jonge, B Smit. The shape selectivity of paraffin hydroconversion in TON, MTT and AEL-type sieves. J Catal 188:403–412, 1999.
44. TLM Maesen, M Schenk, TJH Vlugt, B Smit. Differences between MFI-and MEL-type zeolites in Paraffin Hydrocracking. J Catal 203:281–291, 2001.
45. M Schenk, B Smit, TJH Vlugt, TLM Maesen. Shape selectivity in hydrocarbon conversion. Angew Chem Int Ed 40:736–739, 2001.